ISSN 0097-8078, Water Resources, 2012, Vol. 39, No. 2, pp. 184–199. © Pleiades Publishing, Ltd., 2012.
Original Russian Text © Yu.I. Troitskaya, G.V. Rybushkina, I.A. Soustova, G.N. Balandina, S.A. Lebedev, A.G. Kostyanoi, A.A. Panyutin, L.V. Filina, 2012, published in Vodnye Resursy, 2012, Vol. 39, No. 2, pp. 169–185.

HYDROPHYSICAL PROCESSES

Satellite Altimetry of Inland Water Bodies

Yu. I. Troitskaya[a], G. V. Rybushkina[a], I. A. Soustova[a], G. N. Balandina[a], S. A. Lebedev[b], A. G. Kostyanoi[c], A. A. Panyutin[d], L. V. Filina[d]

[a] *Institute of Applied Physics, Russian Academy of Sciences, ul. Ul'yanova 46, Nizhnii Novgorod, Russia*
[b] *Geophysical Center, RAS, ul. Molodezhnaya 3, Moscow, Russia*
[c] *Institute of Oceanology, RAS, Nakhimovskii prosp. 36, Moscow, Russia*
[d] *Nizhegorodskii Center for Hydrometeorology and Environmental Protection, ul. Beketova 10, Nizhnii Novgorod, Russia*

Received February 2011

Abstract—An algorithm is proposed for determining water level in inland water bodies and coastal zones of seas and oceans. The algorithm was tested for the water area of the Gorki Reservoir, for which radioaltimeter databases show considerable data losses. A model was constructed, describing the shape of a mean impulse reflected from a statistically heterogeneous piecewise-constant underlying surface (topographic model). The model was used to substantiate criteria for data choice for the Gorki Reservoir and to construct a regional algorithm for estimating water level using data from Jason-1 satellite and based on the analysis of the shape of telemetric impulses (retracking). Water level was calculated with the use of an algorithm of regional adaptive retracking Sensor Geophysical Data Record databases for the Gorki and Rybinsk reservoirs. Algorithm application has been shown to considerably increase the amount of actual data and significantly improve the accuracy of water level evaluation. The general principles of retracking of a complex domain (a coastal zone, an inland water body, etc.) are discussed. The principles are based on the calculation of signal with allowance made for the roughness of the reflecting surface and they can be applied to different geographic regions.

Keywords: hydrology, satellite altimetry of inland water bodies, retracking.

DOI: 10.1134/S009780781202008X

INTRODUCTION

Satellite altimetry is an important active method for monitoring the dynamic topography of the World Ocean, enabling one, in particular, to evaluate the height of surface waves and driving-wind velocity. The satellite altimetry method was first developed for the conditions of open ocean at distances from the shore not less than 20 km [12, 7, 15, 6, 32], where it ensures the stated measurement accuracy. Satellite altimetry measurements have been carried out on a regular basis since the mid-1980s. The most important programs are the series of Russian satellites GEOIK (9 satellites), satellites of European Space Agency ERS-1, ERS-2, ENVISAT, as well as TOPEX/Poseidon (T/P) and Jason-1, 2 satellite operating under international program of World Ocean surface topography monitoring. Databases of input altimetry data T/P (operation period from 1992 to 2002), Jason-1 (operation period from 2002 up to the present), and Jason-2 (from 2008 up to the present) are available for free at sites [6] and [35].

The possible applications of satellite altimetry to the monitoring of the coastal zone, inland water bodies (lakes, rivers, and reservoirs), and land surface have been actively discussed in the recent years [4, 18, 29, 34]. Such measurements have been successfully used to determine the topography of the ice cover in Greenland and Antarctic, the roughness and thickness of ice cover [29, 36], and various methods have been proposed to monitor inland water bodies, such as large lakes, reservoirs, inundated territories, and large rivers [3, 16, 25, 26]. Recent studies have shown that the satellite altimetry allows one to measure the elevation of water surface with an accuracy of up to tens of centimeters not only for lakes, but also for large rivers in South America, such as the Amazon [10, 13], Parana, Paraguay, and Uruguay [11, 30], and large Siberian rivers [27]. The hydrological regime of the lower Volga was studied from January 1992 to December 2003 with the use of satellite altimetry, and the obtained results showed good agreement with observational data from gauging stations [1]. Nowadays, the Laboratory of Satellite Geophysical and Oceanographic Studies (LEGOS, Toulouse, France) is implementing a program of water level monitoring in several large reservoirs.

However, the methods for altimetry data processing that have been developed for open ocean, such as retracking algorithm Ocean-1, 2 [20], which are used to produce the main user product of satellite altimetry Geophysical Data Record (GDR), are commonly inapplicable to inland water bodies with linear dimensions of less than 10 km [8, 21, 2]. Examples of such water bodies include the majority of reservoirs, whose

lake parts are commonly elongated along river channels.

The problems of processing altimetry data for inland water bodies are very similar to those arising in attempts to monitor the coastal zone of oceans and associated, primarily, with the distortion of telemetry signal when it reflects from land surface and onshore structures [21]. Because of this, the recovery of parameters for inland water bodies requires special retracking algorithms, which take into account the effect of land. Special retracking algorithms are also required for the recovery of the properties of underlying ocean surface [31, 17]. Thus, examples are known of successful application of satellite altimetry with the use of algorithms Ice-1,2 for determining the thickness of Antarctic and Greenland ice sheets [28, 36] for evaluating snow cover parameters in Canada [33], for global classification of the properties of underlying surface (desert, mountain massifs, forests, wetlands, etc.) [9].

Considerable problems arose in attempts to use satellite altimetry data to monitor the Gorki Reservoir, which has a maximal width of 14 km and steep shores 10–20 m in height. Under such conditions, only a small portion of reflected impulses satisfies the reliability criteria Ocean-1,2, resulting in a considerable loss of data in GDR bases of Jason-1,2 satellites and making the results of data processing unreliable. As the result, the data on water level, essential wave height, and specific effective cross-section of scattering of water surface σ_0 for the Gorki Reservoir, as well as some other Volga reservoirs, were not included in LEGOS database [22] and the database of US Department of Agriculture (USDA-FAS) [23], which contain data on the major lakes and reservoirs, including those in RF territory.

This paper briefly gives the fundamentals of satellite altimetry of ocean and proposes methods of adaptive tracking of altimetry data for relatively small inland water bodies. Those methods are based on the analysis of the shape of reflected telemetric impulses and the application of threshold retracking algorithms. Also given are the results of the application of such methods to the data from Jason-1 altimetry satellite for the Gorki Reservoir and the coastal zone of the Rybinsk Reservoir. The application of adaptive-retracking method considerably reduced the amount of data involved in water level monitoring and radically improved the correlation of results with data of ground-based observations. The general principles used for the construction of regional algorithm can be used for altimetry measurements in the coastal zones of seas and oceans.

THE PRINCIPLES OF SATELLITE ALTIMETRY OF OPEN OCEAN

The method of satellite altimetry is based on evaluating the elevation of sea surface h relative to the reference spheroid by the delay in the arrival time of a sounding impulse reflected from the underlying surface. The satellite altimetry also allows one to measure driving-wind speed and significant wave height.

The problems of studying the dynamic topography of ocean surface, which were meant during the construction of radio altimeters of T/P and Jason-1,2 series satellites, required the spatial resolution of the elevation of sea surface of not more than 5 km, which amounts to 1/10 of the Rossby deformation radius in the ocean for temperate latitudes. Such resolution could be attained by reducing antenna beam width of the radio altimeter. Estimates show that the resolution of 5 km can be attained at microwave radiation wavelength of 2 cm, satellite height of 1000 km, and a large antenna diameter of 5 m. In this case, the antenna beam width is small (~0.004), resulting in large errors associated with the determination of nadir point position. Thus, a deviation of antenna by 0.04 causes an error of 20 cm in the evaluation of height [14]. Those drawbacks can be eliminated by using radio altimeters with relatively wide beam (1°–2°). In this case, the high spatial resolution can be attained by using short telemetry impulses.

When radio waves reflect from diffuse oceanic surface, the signals arriving from its different parts add up incoherently (in terms of power), and the arriving signal is proportional to the illuminated area. Since the height of radioaltimeter above the surface is many times greater than the linear size of the radiating antenna, the signal reaches the Earth surface as a short-time impulse of a spherical wave. As the impulse is propagating, the area of the illuminated area increases in proportion to time within an interval equal to the duration of the sounding impulse, after which it remains unchanged. The power of the arriving reflected impulse signal increases in proportion to the area. The distance from the surface is evaluated from the position of half-width of the leading edge of the impulse. The spatial distribution of the method is $R_0 = \sqrt{hc\tau_i}$ (h is the height of the satellite orbit, c is light speed, τ_i is the duration of the impulse emitted by altimeter antenna), i.e., the shorter the impulse, the better the spatial resolution. In the case of Jason-1,2 satellites, with impulse duration $\tau_i = 3.25$ ns and orbital height $H = 1300$ km, the spatial resolution is ~700 m.

The algorithm for determining underlying-surface parameters is based on approximation of the shape of the signal received by the altimeter by a well-known Brown formula [12], derived from a model of incoherent dispersion of radio waves by a rough surface. Assuming the waves arriving from different parts of the surface to add up incoherently (in terms of power), G.

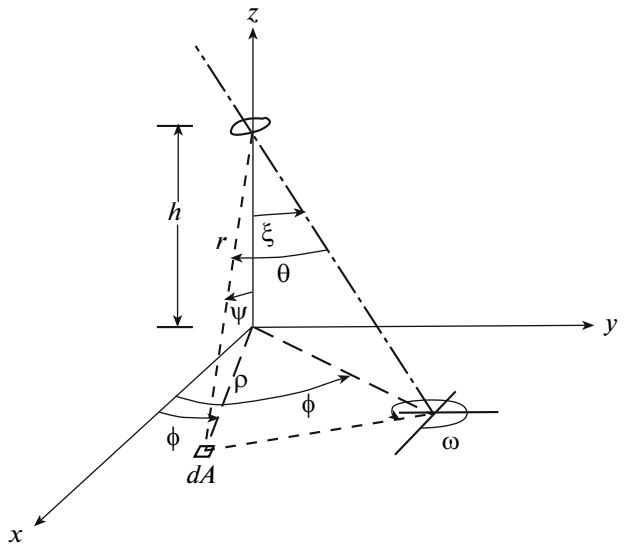

Fig. 1. Problem geometry.

Brown, D. Barrick, and B. Lipa [12, 7] showed that the power of the reflected signal is

$$P_i(t) = P_0 \iint\limits_{\substack{\text{Illuminated}\\ \text{area}}} \frac{G^2(\theta)\sigma(x,y,\theta)}{r^4} dA \times \times \int\limits_{-\infty}^{\infty} p\left(t_1 - \frac{2r}{c}\right) q\left(x, y, \frac{c}{2}(t - t_1)\right) dt_1, \quad (1)$$

where $G(\theta)$ is antenna directional diagram (θ is the angle between antenna axis and the direction to the surface element dA, Fig. 1), r is the distance from the antenna to the elementary area dA on the surface, $p(t)$ is the shape of the emitted impulse, h is the mean distance from the satellite to the surface, σ is the scattering cross-section per unit area, $q(z)$ is the probability density of the height of mirror (scattering) points.

The transformations given in [12] for the case of small-angle approximation and a small deviation of altimeter antenna axis from the nadir ($\theta \ll 1$ and $\xi \ll 1$, Fig. 1), as well as model expressions for antenna directional diagram $G(\theta) = \exp(-2\sin^2\theta/\gamma)$, probability density of the distribution of mirror points $q(z) = \frac{1}{s\sqrt{2\pi}} \times \exp(-z^2/2s^2)$, backscatter cross-section $\sigma = \sigma^{(0)} e^{-\alpha\tan^2\theta}$ and the shape of the sounding impulse $p(t) = \frac{1}{\tau_i\sqrt{2\pi}}\exp(-t^2/2\tau_i^2)$ yield the following expression for the shape of the signal reflected from an infinite homogeneous underlying surface:

$$P\left(t - \frac{2h}{c}\right) = \frac{P_0\sigma^{(0)}}{2h^4} e^{-\left(\frac{4}{\gamma}+\alpha\right)\frac{(ct-2h)}{h}} \times \left(1 + \operatorname{erf}\left(\frac{(ct-2h)}{\sqrt{2}\sqrt{s^2 + c^2\tau_i^2}}\right)\right) \exp\left[-\frac{4}{\gamma}\sin^2\xi - \frac{c}{h}\right. \quad (2)$$
$$\left. \times \left(t - \frac{2h}{c}\right)\left(\frac{4}{\gamma}\cos 2\xi + \alpha\right)\right] I_0\left(\frac{4}{\gamma}\sin 2\xi\sqrt{\frac{c}{h}\left(t - \frac{2h}{c}\right)}\right).$$

In the model expressions used here, parameters s and τ_i characterize the mean roughness height of the underlying surface and the duration of the sounding impulse, respectively.

Figure 2 gives the shape of the impulse described by formula (2) [12], which is commonly used to approximate the signal reflected by water surface in an open ocean (in standard algorithms Ocean-1,2). In this figure, a unit (a telemetric gate) corresponds to the time interval of 3.125 ns; note that in the standard processing algorithm, the arrival time of the reflected signal is assumed the 32nd gate of this plot.

The shape of the reflected impulse approximated by Brown formula in algorithms Ocean-1,2 is used to determine the impulse's major characteristics: t_0, the mean time lag of the impulse reflected from water surface; τ_0, the width of the leading edge; and $A_{\max}$, the maximal power value (Fig. 2), which allow one to evaluate the height of satellite orbit above water surface $h = t_0 c/2$, the significant wave height SWH = $2s$ and the backscatter cross-section, which in the case of sea surface, reflects mostly on wind speed and SWH. Sea surface height SSH can be found as

$$\text{SSH} = \text{Altitude} - \text{Orbit} - \text{Corrections}, \quad (3)$$

where Altitude = h is satellite orbit height over water surface; Orbit is satellite orbit height over the reference spheroid; Corrections are corrections for the state of the atmosphere, the state of the underlying surface, tides, etc., which affect the signal arrival time [6, 32]. The errors in evaluating those and other parameters (wind speed, significant wave height, backscatter cross-section, etc.) for the conditions of open ocean are given in [6]. The high accuracy of altimetry measurements is attained through the averaging of a large number of unit, strongly irregular telemetric impulses over a time interval of 1 s [6, 32]. Note that within this time, the nadir point sifts by 5.8 km, and the stated measurement accuracy is attained in this case. At the same time, the minimal spatial resolution of satellite altimeter data, determined by the duration of the telemetric impulse, is ~700 m (as mentioned above). The time interval of repetition of measurements along the tracks of satellites T/P and Jason-1,2 is 9.916 days.

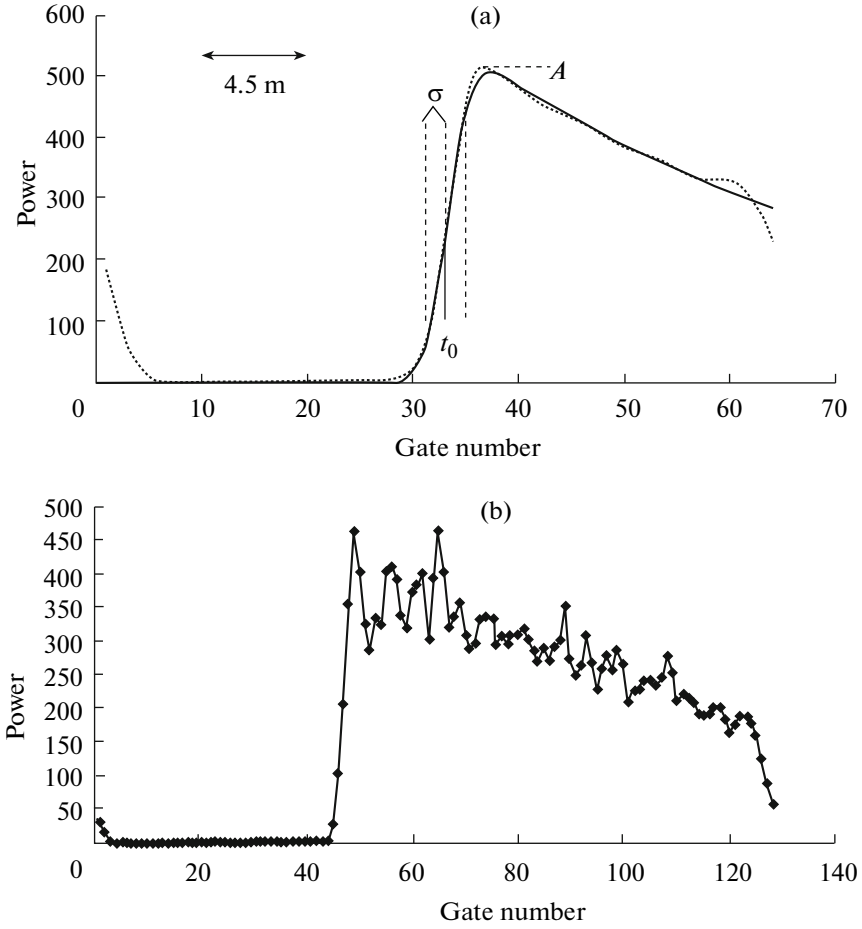

Fig. 2. (a) The shape of impulse reflected by an infinite underlying surface according formula (2) [12] and (b) the shape of an averaged altimetry impulse for open ocean.

SPECIFIC ASPECTS OF ALTIMETRY OF INLAND WATER BODIES. FUNDAMENTALS OF THE METHOD OF ADAPTIVE REGIONAL RETRACKING

The shape of telemetry impulses, received by altimeter antenna, is significantly different, depending on whether they form in the coastal zone or in the open ocean. This is due to the effect of reflection from the land. Figure 3 gives examples of telemetric impulses that form due to combined reflection from land and water (Fig. 3a), quasimirror, coherent reflection from water surface at mouths and in harbors (Fig. 3b), and from other strongly reflecting objects (near-shore structures, large-area slicks, etc.) (Fig. 3c).

Impulses with additional peaks are difficult to approximate by Brown formula, hence an error in the determination of leading front position of the impulse and incorrect calculation of the height of the satellite above water surface and water surface level. Other characteristics, such as wind speed and wave height, are also evaluated with errors. Because of this, special algorithms have been actively developed in recent years for processing altimetry data in coastal zones [4, 18], large rivers [3, 10, 11, 13, 25, 27, 30], and lakes [1, 8, 16, 26]; however, there still is no single regular procedure allowing one to use satellite data for successful evaluation of water level in the cases where reflection from land significantly affects the shape of the arriving telemetry impulses. The arrival time of reflected impulse can be determined by different retracking algorithms, e.g., threshold retracking, β-retracking [17, 18, 31], etc. In this study, we suggest a method of regional adaptive retracking based on the construction of a theoretical model describing the formation of telemetric impulse due to reflection from a piecewise constant model surface (Fig. 4) and taking into account the geographic features of the region. The model is used as the basis for formulating the criteria for selection of telemetric impulses and substantiating the applicability of a threshold and improved threshold-retracking algorithms for evaluating the characteristics of underlying surface in an inland water body. Next, the possible application of those methods for the Gorki and Rybinsk reservoirs in the Volga River is demonstrated.

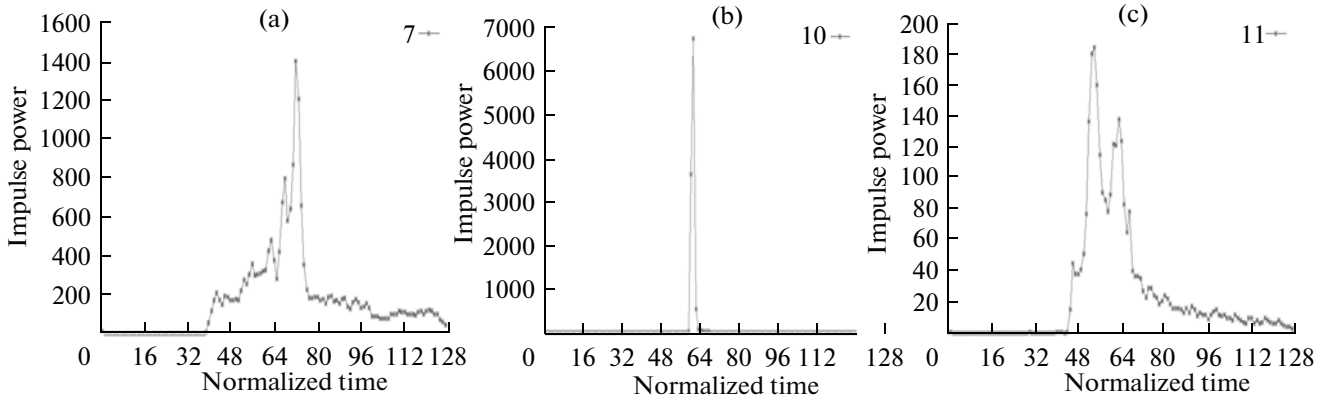

Fig. 3. The shapes of impulses in the coastal zone and in an inland water body. (a) Joint reflection from land and water. (b) Quasimirror, coherent reflection from water surface in mouths and harbors. (c) The presence of several strongly reflecting objects.

Suppose that the illuminated area on the underlying surface is comprises several parts with different elevations and reflecting properties. Figure 4 gives an example of such surface near the 142nd track of Jason-1 satellite in the Gorki Reservoir with its piecewise constant approximation. Water, slicks, and land are shown in different colors. Suppose that the antenna axis is directed strictly to nadir ($\xi = 0$). With the accepted model expressions for surface and antenna characteristics and with change to polar coordinates for integration over the illuminated surface, formula (1) becomes

$$P_i(\tau) = \frac{P_0}{\sqrt{2\pi}h^4}\int_0^{\infty}\int_0^{2\pi}\frac{\sigma^{(0)}(\rho,\varphi)}{s(\rho,\varphi)}e^{-\left(\frac{4}{\gamma}+\alpha(\rho,\varphi)\right)\frac{\rho^2}{h^2}} \times \exp\left\{-\frac{\left(c\tau - 2H(\rho,\varphi) - \rho^2/h\right)^2}{8s^2(\rho,\varphi)}\right\}\rho d\rho d\varphi, \quad (4)$$

where $H(\rho,\varphi)$ is the deviation of the elevation of underlying surface from its mean level. In the case of a rough surface, the parameters in (4) are functions of coordinates. However, in the case of a piecewise constant model (Fig. 4), those parameters are constant within each part of the surface, and integration over each part yields

$$P_k(\tau) = \frac{P_0\sigma_k^{(0)}}{4\pi h^4}e^{-\left(\frac{4}{\gamma}+\alpha_k\right)\frac{(c\tau-2H_k)}{h}}\left(1+\operatorname{erf}\left(\frac{(c\tau-2H_k)}{2\sqrt{2}\sqrt{s_k^2+c^2\tau_i^2}}\right)\right) \times \Delta\varphi_k\left(x_N, y_N, \sqrt{h(c\tau-2H_k)}\right), \quad (5)$$

where variables with subscripts k: $\sigma_k^{(0)}$, α_k, s_k correspond to the parameters of scatter and roughness for the given (kth) part of the underlying surface. As can be seen from (5), the contribution of each part of the surface to reflection can be described by an analogue of Brown formula ((2) with $\xi = 0$). Unlike Brown formula, where, because of the homogeneity of the surface, integration over the angle φ yields the factor 2π, the formula for the piecewise constant model (5) contains the factor $\Delta\varphi_k(x_N, y_N, \sqrt{h(c\tau - 2H_k)})$. This means that at the moment τ, the reflection is due to the arc of circumference $\Delta\varphi_k$((Fig. 4) with the center in the nadir point, with coordinates x_N, y_N, and radius $\sqrt{h(c\tau - 2H_k)}$, corresponding to the distance from nadir point, from which the reflected signal from that

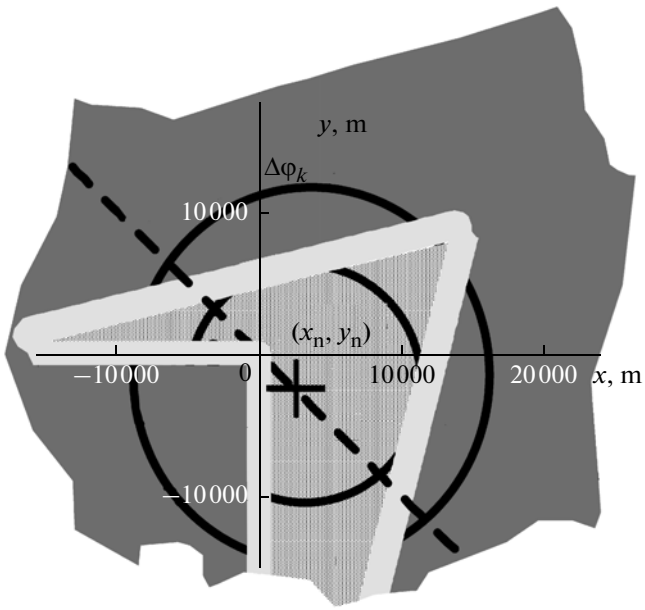

Fig. 4. Piecewise constant model of the underlying surface of the Gorki Reservoir near Yur'evets Town in the vicinity of the 142nd track of Jason-1,2 and T/P satellites (+ marks the position of nadir point, the dashed line is satellite trajectory, the circumference is the boundary between the illuminated domain in the given moment, the dotted area is water surface, the dark gray area is land surface, the light gray areas are coastal slicks).

part of the underlying surface arrives to the antenna (this radius also depends on the deviation of the elevation of this part of the surface H_k from the mean level). The total reflected power is the sum of powers reflected from all parts of the surface

$$P(\tau) = \sum_K P_K(\tau). \quad (6)$$

Using formulas (5), (6), one can evaluate the waveforms of reflected altimetry impulses and their change during satellite motion along the track.

AN EXAMPLE OF THE USE OF SATELLITE ALTIMETRY FOR DETERMINING WATER LEVEL IN THE GORKI RESERVOIR

Problems Arising in the Determination of Water Level in the Reservoir Using Data of GDR Jason-1

The Gorki Reservoir, one of the 9 reservoirs of the Volga chain, is situated in the upper part of the Volga basin. The lake-type part of the Gorki Reservoir is 97 km in length, from 3 to 14 km in width, and up to 22 m in depth. Notwithstanding its relatively small size, the reservoir water area is crossed by tracks of several altimetry satellites, including T/P, Jason-1, Jason-2, ERS-1, ERS-2, ENVISAT, GEOSAT, and GFO-1 (Fig. 5). In this study, we use for the analysis the altimetry data of the 142nd track of T/P and Jason-1 satellites. In addition to the important advantage of availability of altimetry data [6], those satellites provide a continuous and the longest series of measurements (since 1992 up to now); a small recurrence orbital period (~9.916 day), which is close to the characteristic time scale of hydrological phenomena; and the possibility to compare with data from the gage at Yur'evets weather station.

Because of the small width of the Gorki Reservoir (up to 14 km), from the viewpoint of satellite altimetry, its territory can be considered as a coastal zone; therefore, there are almost no altimetry data of standard spatial resolution (5.8 km), obtained by averaging over 1 s intervals. That is why, at the first stage, the authors processed the available data of high spatial resolution from GDR bases of Jason-1 satellite (the averaging frequency 20 Hz). The calculations took into account all necessary corrections [5, 32], i.e., for the effect of the atmosphere and ionosphere, and for tides in the Earth crust. The correction for the effect of the atmosphere due to the scatter of radio impulses by molecules of air gases ("dry" atmospheric correction) and the correction for air humidity were derived from the data of European Centre for Medium-Range Weather Forecasts (ECMWF). Note that the corrections for air humidity for the determination of the levels of seas and oceans are commonly calculated with the use of data of space-borne multichannel radiometer. This approach is inapplicable in the case of inland water bodies because of the large size of the underlying surface segment from where radiation is received (more than 40 km) and which is commonly much larger than the size of the water body. The use of the ionosphere correction calculated based on data of double-frequency altimeter is also difficult in the case of inland water bodies because of the nonstandard shape of impulses reflected by land surface partially covered by water or ice. The correction for tides in the Earth crust was also taken from model calculations. The "inverse barometer" corrections, as well as corrections for the state of underlying surface, oceanic, and polar tides, which are used in determining ocean level, were not used in the case of continental waters. A similar procedure was used in LEGOS [22] to determine the hydrological regime of major rivers of South America, Africa, and Siberia and in the Geophysical Center, RAS, for determining water level in the Lower Volga.

The results of calculations of water level variations in the Gorki Reservoir based on data of Jason-1 satellite from 2002 to 2008 by a standard algorithm are given in Fig. 6a. Data of measurements at the gauging station at Yur'evets weather station are also shown in this figure. Notwithstanding the good agreement between data of satellite altimeter measurements and in-situ data from Yur'evets gauging station for the Gorki Reservoir, it can be noted that the data of remote sounding show a wide scatter (Fig. 6). Figure 6b shows the dependence of standardized deviations of water level based on satellite data from standardized in-situ data and the best linear approximation of this dependence with the slope $K = 0.33$ equal to the correlation coefficient between the altimetry and in-situ data. The low correlation between the satellite and in-situ measurements is due to the considerable losses of data and considerable errors, caused by drawbacks of the direct application of algorithms for the calculation of the height of water surface developed for large-area water bodies (oceans and seas) to medium-area water bodies, in which the illumination domain within the antenna directional diagram of radio altimeter largely lays on the land. It is also worth mentioning that the hydrometeorological regime of the Gorki Reservoir shows strong seasonal variations. In winter (November–April), the lake-type part of the reservoir is covered by ice and snow; the mean freeze-up date is November 22 (between November 7 and December 7). In summer (May–October), the water area is free of ice; the mean date of the lake-type part of the reservoir becoming free of ice is May 3 (between April 18 and May 18).

To elucidate the causes of significant errors, we analyzed the shapes of altimetry impulses for the 142nd track of Jason-1 satellites in the zone of the Gorki Reservoir. The required data were taken from SGDR database of Jason-1 satellite. Figure 7 gives the shapes of "winter"(March 25, 2005) and "summer" (June 5, 2006) 20-Hz telemetric impulses for the 142nd track of Jason-1 satellite in the zone of the Gorki Reservoir. Analysis of impulse shapes has shown

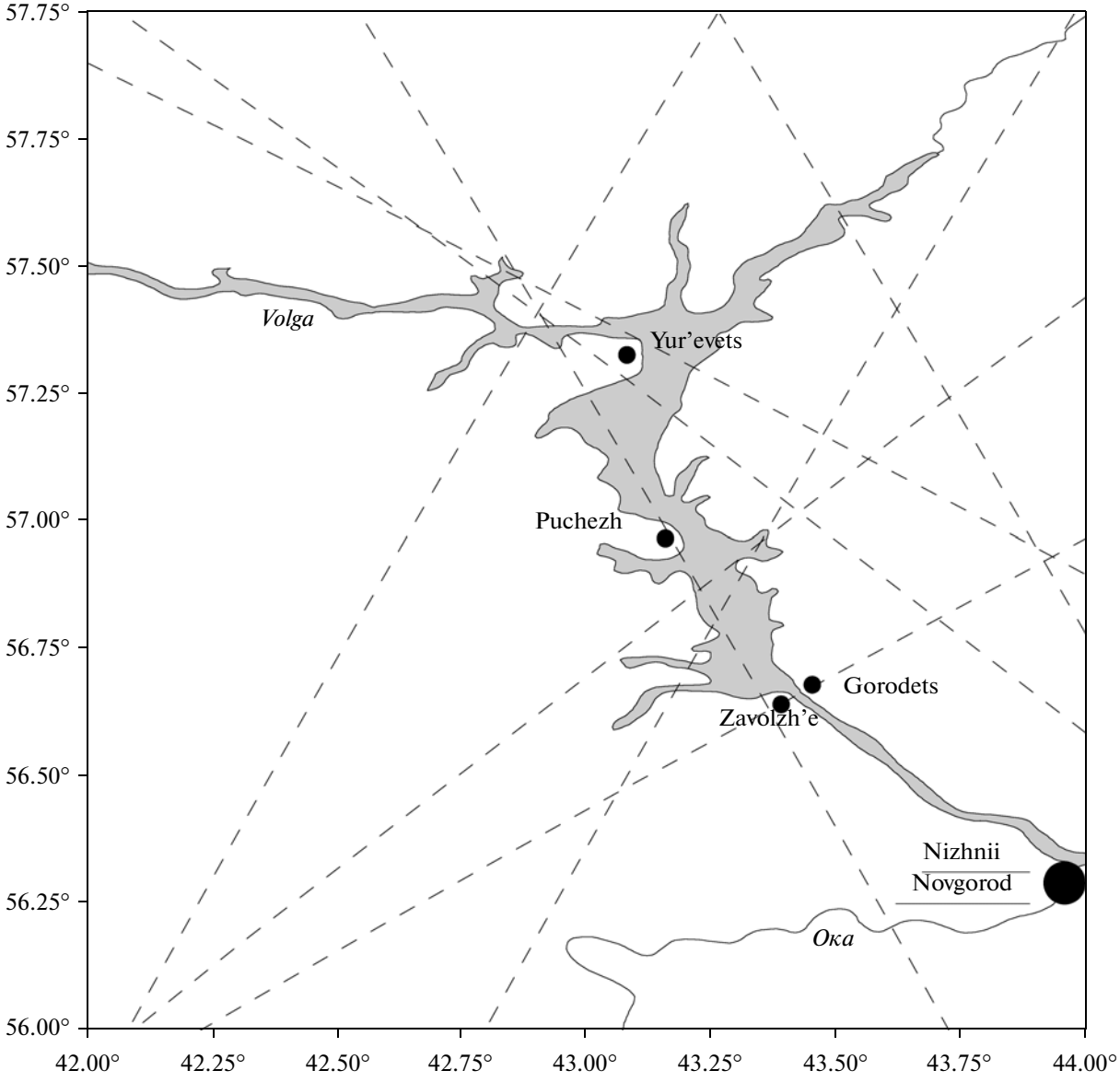

Fig. 5. The passage of slicks of altimetry satellites over Gorki Reservoir water area.

that "winter" impulses are more regular and they can be treated with better accuracy by the well-known retracking algorithms (Ice-1,2 [4, 29]), while "summer" impulses have several peaks with anomalous amplitude. We can suppose that the scatter of data on water level is due to the drawbacks of the calculation algorithm use in GDR, where the telemetric impulse is approximated by Brown formula [12], and the arrival time of reflected signal is taken to be the 32nd gate. The reflected signal can be shifted in time, and the 1-gate error(3.125 ns) does not lead to a considerable error in water level measurement (it is of the order of $dt_i c/2$, or ~0.5 m). Thus, the algorithms used for medium-size water bodies should take into account the effect of reflection from land, associated coastal slicks, and other strongly reflecting objects on the shape of telemetric impulses.

Calculation of the Shape of Telemetric Impulses Based on Piecewise Constant Model of the Underlying Surface Near the Gorki Reservoir

The first step in the development of a retracking algorithm is the evaluation of the shape of telemetric impulses based on a simplified piecewise constant model of underlying surface (Fig. 4). It is worth mentioning that, during the field studies, we identified a specific feature of Gorki Reservoir water area, which could have a significant effect on the shape of the reflected impulses. Smooth areas 20–30 m in width (slicks) were often observed near reservoir shores.

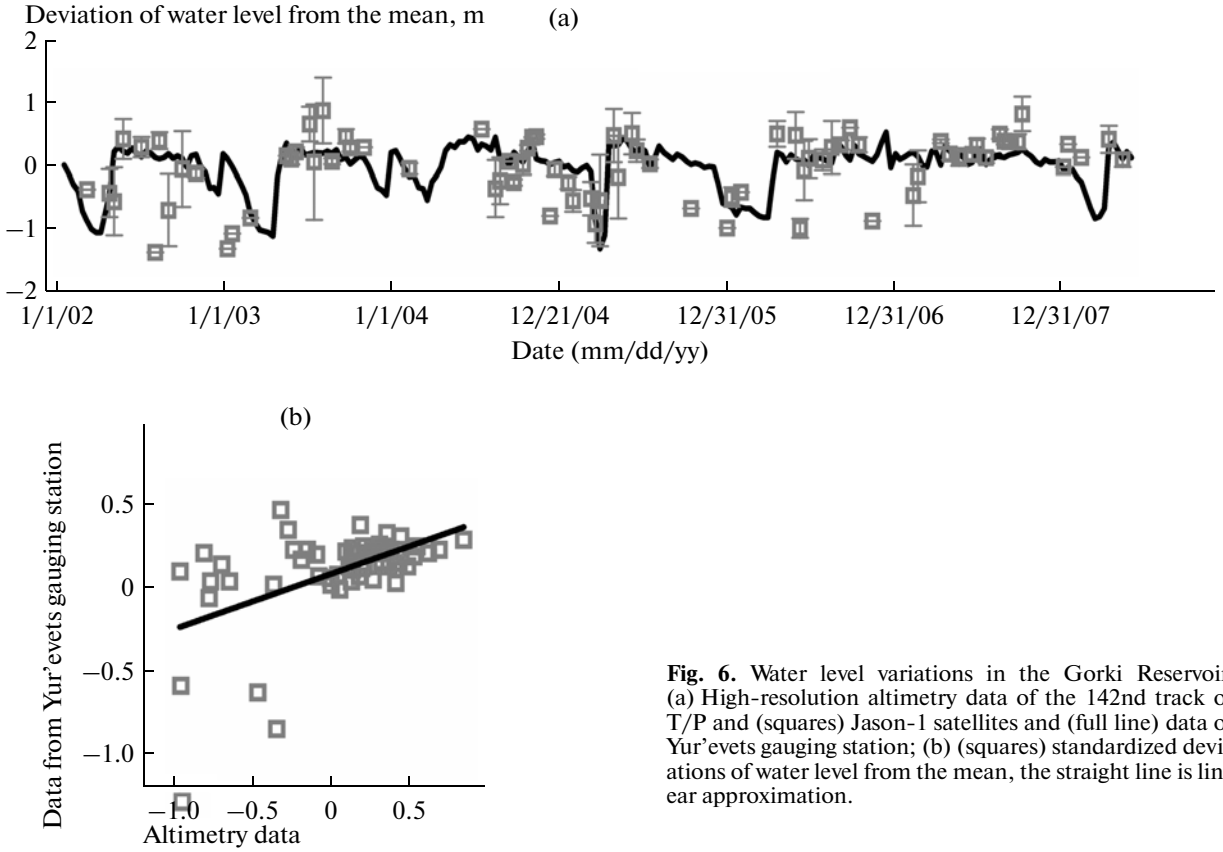

Fig. 6. Water level variations in the Gorki Reservoir. (a) High-resolution altimetry data of the 142nd track of T/P and (squares) Jason-1 satellites and (full line) data of Yur'evets gauging station; (b) (squares) standardized deviations of water level from the mean, the straight line is linear approximation.

Those slicks may be due to the high concentrations of surfactants associated with economic activity. The presence of slicks is known to be a cause of peaks in telemetric impulses [38].

The contribution of slicks to reflection can be evaluated from (4) with the assumption that the slick domain is a narrow strip with a width of d_{sl}, whose position is specified by the equation of coastal line $y = y(l)$, $x = x(l)$. Now the power dissipated by slicks is described by

$$P_{sl}(\tau) = \frac{P_0 \sigma_{sl}^{(0)} d_{sl}}{\sqrt{2\pi} h^4 s_{sl}} e^{-\left(\frac{4}{\gamma}+\alpha_{sl}\right)\frac{c\tau-2H_{water}}{h}} \times \int_C e^{\left\{-\left(c\tau-2H_{water}-\frac{(x(l)-x_N)^2+(y(l)-y_N)^2}{h}\right)^2 \Big/ 8s_{sl}^2\right\}} dl. \quad (7)$$

Because of the smoothness of water surface in a slick, $S_{sl} = c\tau_i$, and the values of dissipation parameters $\sigma_{sl}^{(0)}$ and α_{sl} in a slick are much greater than their values for wave-covered water.

The reflected power received by altimeter antenna is the sum of contribution to the reflection of water and land (their contributions can be described by (5)), as well as of coastal slicks

$$P(\tau) = P_{water}(\tau) + P_{land}(\tau) + P_{coast}(\tau), \quad (8)$$

where $y = y(l)$, $x = x(l)$ is shoreline equation. Equations (5), (7), and (8) can be used to describe the model shapes of impulses for a piecewise constant model of underlying surface near the Gorki Reservoir.

The parameters in (5), (7) are determined by the properties of the surface. Thus, for reservoir water area, the height H is water level, parameter s is determined by the significant wave height SWH, σ characterizes the dissipating properties of water surface and depends on wind speed. For land surface near the reservoir, the height H is determined by land topography, s is determined by land surface roughness, and σ depends on the reflecting properties of the land. In the construction of the model, land parameters are assumed constant, while water surface characteristics (water level, wave height, and roughness) are variable and they should be determined with the use of retracking algorithm.

The solution of the direct problem of determining the shape of impulses, scattered by the underlying surface requires estimation of the typical values of major model parameters in expressions (5), (7) for the region under study.

Data on the topography of land surface near the Gorki Reservoir were taken from database on Earth land surface with a resolution of 1 km (Global Land One-km Base Elevation Project (GLOBE)) [24]. The land topography and sections near the 142nd track of

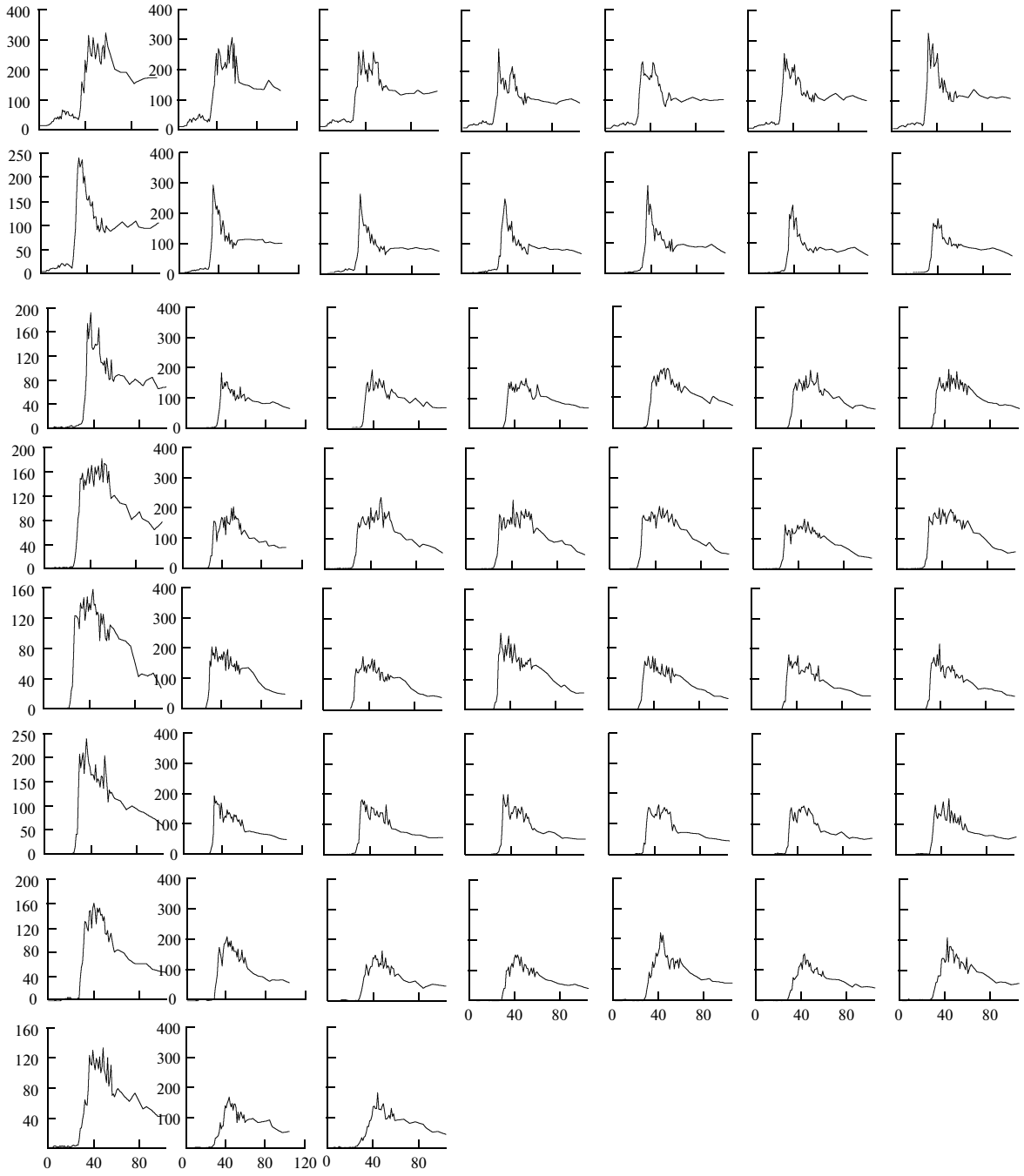

Fig. 7. Telemetric impulses near the Gorki Reservoir (a) in winter (March 25, 2005) and (b) in summer (June 5, 2006).

Jason-1,2 are shown in Fig. 8. According to GLOBE data, the heights of the high (right) and low (left) shores are ~30–50 and 20 m, respectively.

In the modeling of the contribution to the shape of telemetric impulses due to reflections from water surface, water level in the reservoir was assumed spatially homogenous. To evaluate s, we needed estimates of the essential height of wind waves, which were derived from data on wind speed and direction collected at Yur'evets weather station (57°20′N, 43°07′E). It is worth mentioning that wind speed in reservoir water area is not equal to that measured at an onshore weather station. Special field measurements showed wind speed in water area to be 1.5–2.0 times greater than that on the shore.

To evaluate the significant wave height, the authors used an empirical relationship, which had been derived from a generalization of field measurements in an inland water body (Lake Ontario) [19]

Fig. 7. Contd.

$$\mathrm{SWH} = 0.2074\frac{U_{10}^2}{g}\Omega^{-1.55}. \quad (9)$$

Here, $\Omega = U_{10}/c_p$ is wave age parameter, U_{10} is wind speed at the height of 10 m, c_p is the phase speed of the peak in wind speed spectrum. As shown in [19], the wave parameter is related to the wave fetch x by the empirical formula

$$\Omega = 22\left(\frac{gx}{U_{10}^2}\right)^{-0.33}. \quad (10)$$

To find the statistics of surface waves, we evaluated the angular distribution of fetches as a function of wind direction for the middle point of the 142nd track of altimetry satellites on reservoir water area. This distribution is anisotropic because of the elongated shape

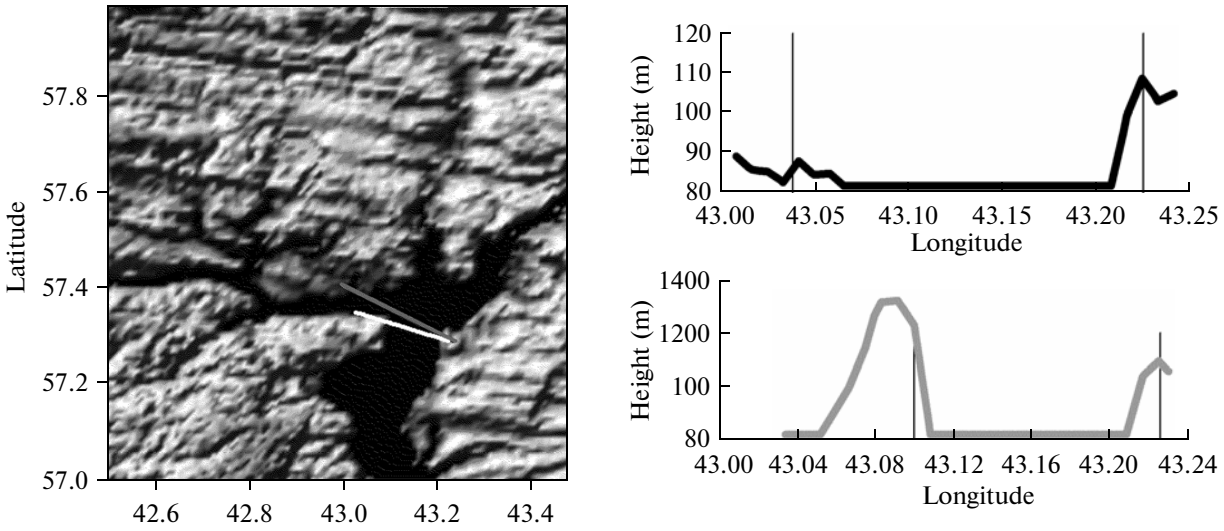

Fig. 8. Land surface topography near the Gorki Reservoir from database [24] (the top right plot corresponds to the dark straight line in the left plot, the bottom plot corresponds to the light straight line).

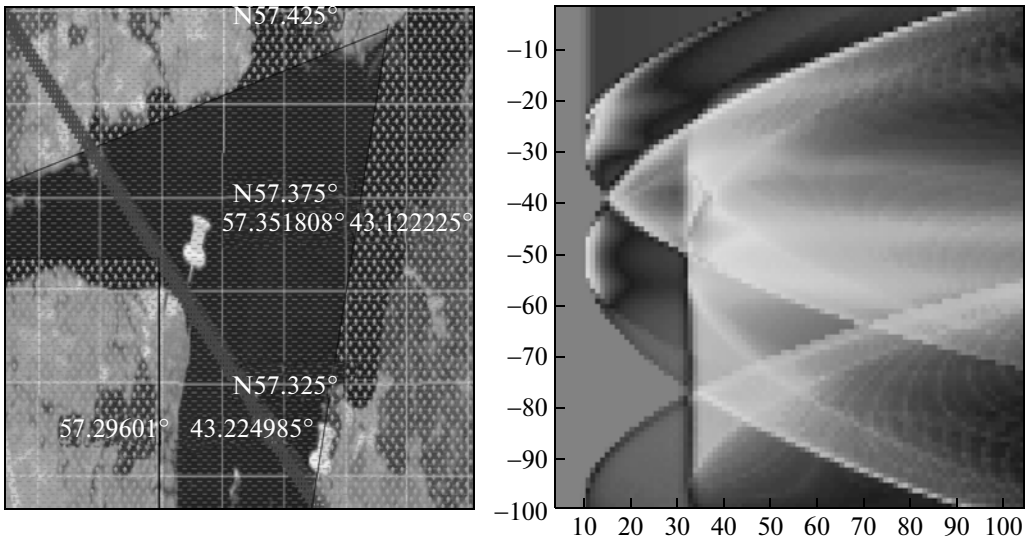

Fig. 9. Model shapes of reflected impulses near the Gorki Reservoir. (a) Referencing of the topologic map to the map of the region, (b) diagram of model wave shapes in coordinates time (horizontal)–distance along the track (vertical).

of the reservoir, the fetch attaining its maximum at southwestern wind.

The distribution histograms of wind speed and direction at Yur'evets weather station (with the use of a coefficient for conversion of wind speed from land to water area) and the histograms of the angular distribution of fetches and formulas (9) and (10) were used to calculate the statistics of significant wave heights in the Gorki Reservoir in summer.

Choosing parameters of model (5), (7), and (8) in accordance with the obtained estimates, the authors calculated the shapes of telemetric impulses. The parameter values taken for calculations were $s = 0.1$ m, $\sigma^{(0)} = 1$, and $H = 20$ m for the land and $s = 0.3$ m, $\sigma^{(0)} = 10$, and $H = 0$ for water. The results of calculations are given in Fig. 9b in the form of projection images of the shapes of telemetric impulses in coordinates time–distance along the track. The time is measured in units of telemetric gates (3.25 ns), and the distance is measured in units of readings along the track (700 m). The complex shape of images reflects the complex shape of calculated model impulses. Their characteristic feature is the specific parabolic shape corresponding to reflection from shores and scatter on smooth zones near shores. The impulses have a very narrow leading edge, because SWH averages 0.28 m, which corresponds to less than 1 telemetric gate.

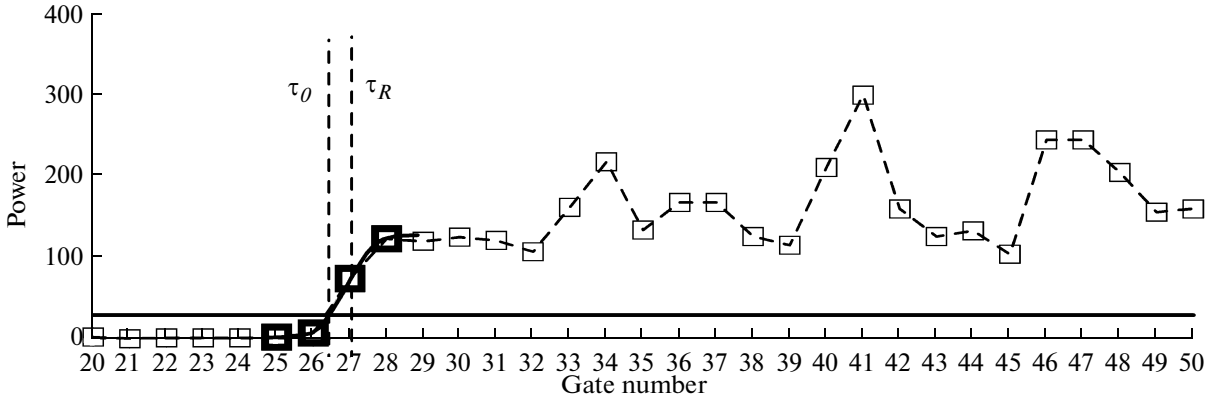

Fig. 10. Example of impulse shape for Jason-1 satellite: cycle 162, track 142, Ku-range (the full line is the threshold power value, τ_0 is threshold retracking, τ_R is improved threshold retracking).

Analysis of the shape of impulses allowed us to formulate criteria for the choice of telemetric impulses: for determining water level, one should take the impulses from the part of the Gorki Reservoir between 43.14 and 43.22°E (the lower part of the diagram in Fig. 9b, corresponding to the domain between labels in Fig. 9a), since it is only in this area that the signal reflected from water can be reliably identified. Moreover, long-term observations at Yur'evets gauging station suggest that, in the Gorki Reservoir, water level deviations from the mean exceeding ±2 m should be regarded as an error.

Once the criteria for impulse selection are determined, a two-step retracking procedure should be implemented. At the first step (threshold retracking), the arrival point of impulse t_0 is determined by the rise above a threshold q_0 (Fig. 10); next, at the second step (improved threshold retracking), four points near the threshold are approximated by the error function

$$A\left(1+\operatorname{erf}\left(\frac{\tau-\tau_R}{S}\right)\right) \qquad (11)$$

and the parameters A, τ_R, and S are determined via an optimization procedure (root-mean-square deviations are minimized). The possibility to approximate the leading front of the part of impulse that is reflected from water surface by the error function has been proved above in the theoretical model. Indeed, the exponent in the right-hand part of (5) is a smooth function relative to the error function erf; therefore, the increase in the impulse power near the leading edge can be assumed to be determined by the error function. The improved retracking algorithm (Fig. 10) gives a more accurate value for the track point (the middle of the leading front of the impulse reflected from water). The difficulties in the application of this method are only due to the choice of an adequate optimization procedure. Note that when the impulse arrival time is determined with the use of algorithm Ocean-1, the obtained track point is placed in the 32nd gate of the plot (Fit. 10), thus leading to a 5-gate error in the arrival time and an error in water level evaluation of 2.5 m.

In conclusion of this section, we formulate the main principles of the developed algorithm of regional adaptive retracking, which can be applied to both inland water bodies and coastal waters:

the development of a piecewise constant topographic model of underlying surface;

the solution of the direct problem of determining model wave shapes;

the formulation of selection criteria of telemetric impulses;

step-by-step solution of the inverse problem by threshold and improved threshold retracking.

APPLICATION OF THE ALGORITHM OF ADAPTIVE REGIONAL RETRACKING TO CALCULATING WATER LEVEL VARIATIONS IN THE GORKI AND RYBINSK RESERVOIRS. THE COMPARISON OF CALCULATION RESULTS WITH MEASUREMENTS AT GAUGING STATIONS

In this section, the method of adaptive regional retracking, whose theoretical principles are given above, is applied to the calculation of water level in the Gorki Reservoir and in the coastal zone of the Rybinsk Reservoir. In accordance with the results of the previous section and the formulated criteria of the choice of altimetry impulses, the impulses for retracking and evaluating water level in the Gorki Reservoir were taken from a part of the 142nd track, corresponding to 43.14°–43.22°. Next, they were subject to two-step processing. At the first step, threshold-tracking algorithm was applied, in which the arrival moment of the reflected impulse was evaluated by the excess over the power threshold. At the same time, the threshold level was varied, and the best results in terms of density were

Water level variance and the number of actual points in summer and winter seasons for different retracking algorithms

Data from GDR database	Root-mean-square deviation		Mean number of actual points per month	
	Winter (November–April)	Summer (May–October)	Winter (November–April)	Summer (May–October)
GDR data	0.15	0.16	0.3	1.2
Threshold method	0.15	0.13	1.5	2.0
Improved threshold method	0.18	0.12	1.5	2.0

obtained were obtained at the level of the order of 30–50 units of dimensionless power. At the second step (improved threshold method) the position of the track point (the middle of the leading front of the reflected impulse) was evaluated more precisely by approximating the leading front (4 gates near the threshold determined at the first step) by the error function (11) and minimizing the mean-square deviations.

The results of calculation of water level in the Gorki Reservoir by the two-step adaptive retracking and their comparison with measurements at Yur'evets gauge and GDR data are given in Fig. 11a. These results were used to calculate the correlation coefficient between altimetry data for the 142nd track of Jason-1 satellite and data of ground measurements (the slope of the straight lines in Fig. 11b) and to find the errors of water level evaluation and the number of actual points in the summer and winter seasons for different retracking algorithms (table). The analysis has shown a considerable increase in the number of reliable measurement points and a significant improvement in the correlation between satellite and ground data. The correlation coefficient between altimetry data and measurements at Yur'evets gauge increased from 0.33 (for data with high spatial resolution from standard Ocean-1 algorithm) to 0.88 for the adaptive retracking method.

The improved threshold method was also used to calculate water level in the Rybinsk Reservoir by

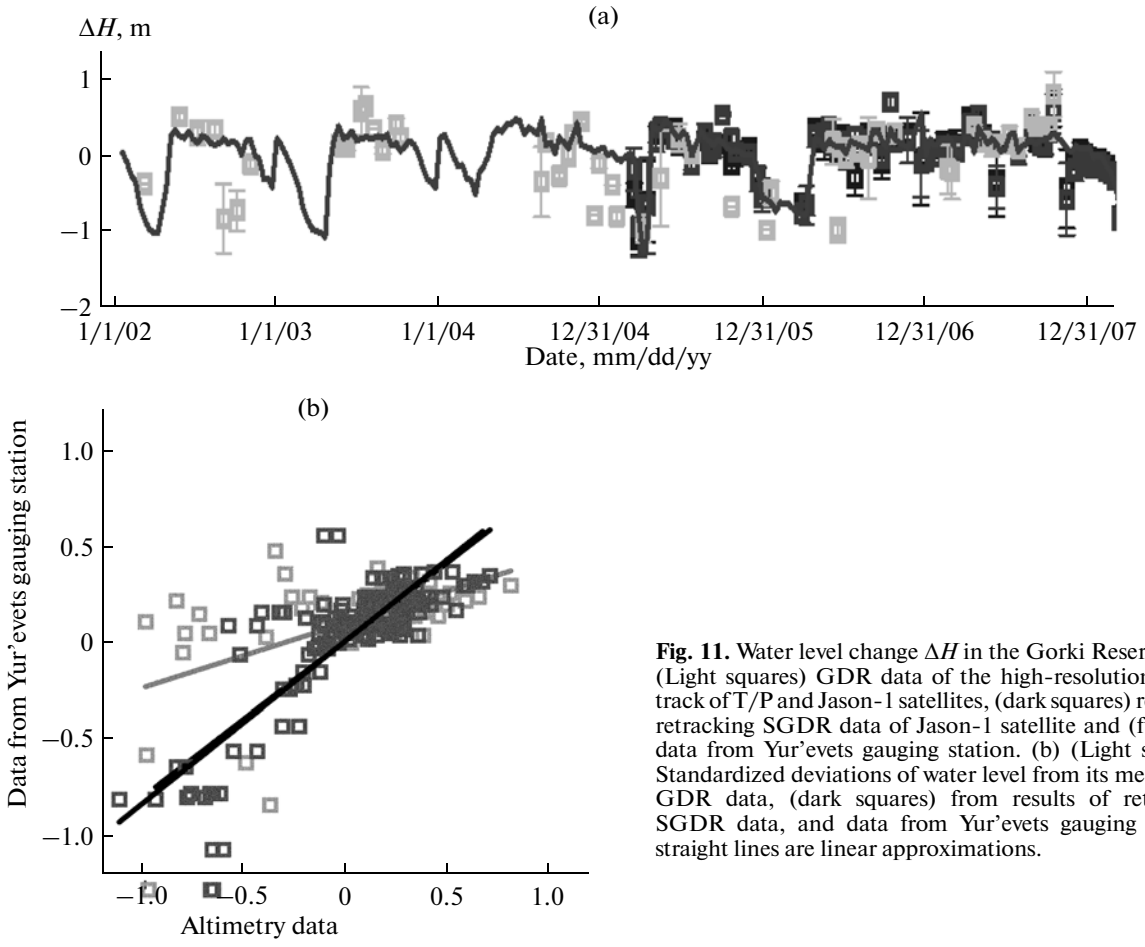

Fig. 11. Water level change ΔH in the Gorki Reservoir. (a) (Light squares) GDR data of the high-resolution 142nd track of T/P and Jason-1 satellites, (dark squares) results of retracking SGDR data of Jason-1 satellite and (full line) data from Yur'evets gauging station. (b) (Light squares) Standardized deviations of water level from its mean from GDR data, (dark squares) from results of retracking SGDR data, and data from Yur'evets gauging station; straight lines are linear approximations.

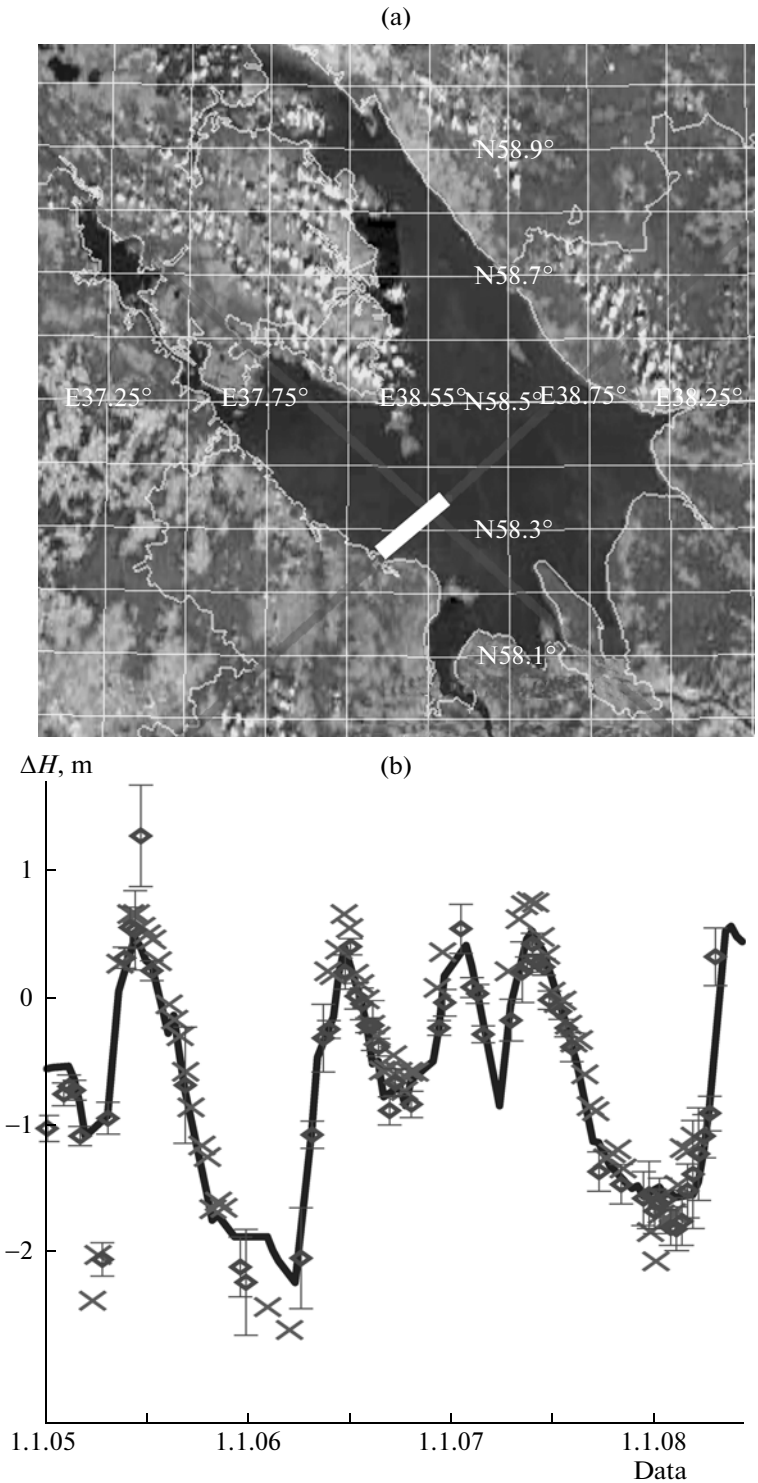

Fig. 12. (a) Map of the area and (b) deviations of water level from the mean ΔH for the Rybinsk Reservoir. (*1*) GDR data of the high-resolution 59th track of Jason-1 satellite, (*2*) results of retracking of SGDR data of Jason-1 satellite, the full line shows the data of Breitovo water level gauge.

altimetry data. Figure 12a gives a map of the Rybinsk Reservoir, and Fig. 12b gives the calculated water levels in the coastal zone of the 059th track of Jason-1 satellite (the light part of the track in Fig. 12a). In this case, retracking also considerably increases the number of actual points (3–4 times as compared with the standard algorithm), and the error in water level evaluation is about 16 cm even for the simple threshold method. This is better than the results for the Gorki Reservoir (where the error of the threshold method

was about 25 cm), because of its simpler topology and larger size. It is worth mentioning that the threshold method also yields good results for the central part of the Rybinsk Reservoir, since in inland water bodies, the leading front of reflected telemetric impulse is very narrow because of the small (as compared with seas and oceans) wave height (there is no swell). Thus, the threshold and the improved threshold methods can be recommended as major instruments for calculating water level in inland water bodies.

CONCLUSIONS

An algorithm is proposed for determining water level in inland water bodies and the coastal zone of seas with an error of the order of 10–15 cm. The algorithm has been tested in a difficult case of the Gorki Reservoir, where the standard algorithm Ocean-1 is inapplicable, resulting in considerable data losses. A model of the shape of a mean impulse reflected from statistically heterogeneous piecewise constant surface (topographic model) is constructed and used to theoretically evaluate the reflected power based on works [12, 7]. The model is also used to substantiate the criteria for data choice for the Gorki Reservoir. Water level was calculated with the use of regional adaptive retracking of SGDR data for the Gorki and Rybinsk reservoirs. It is shown that the application of the algorithm considerably increases the volume of data involved and significantly improves the accuracy of water level evaluation.

The general principles of retracking of a complex domain (a coastal zone, inland water bodies, etc.) are based on the calculation of signal with allowance made for the roughness of the reflecting surface and they can be applied to different geographic regions.

ACKNOWLEDGMENTS

This study was supported by the Russian Foundation for Basic Research and the Government of Nizhegorodskaya province, project no. 08-05-97016-r_povolzh'e_a, and FTsP "Scientific and Scientific-Pedagogical Human Resources of Innovation Russia for 2009–2013, State Contract no. P623 of May 18, 2010.

REFERENCES

1. Lebedev, S.A., and Kostyanoi, A.G., *Sputnikovaya al'timetriya Kaspiiskogo morya* (Satellite Altimetry of the Caspian Sea), Moscow: Izd. tsentr "MORE" Mezhdunar. Inst. okeana, 2005.
2. Troitskaya, Yu.I., Balandina, G.N., Rybushkina, G.V., et al., Studying the Variability of Water Level in the Gorki Reservoir Based on Satellite Altimetry, *Issled. Zemli Kosmosa*, 2010, no. 6, pp. 1–9.
3. Alsdorf, D., Birkett, C., Dunne, T., et al., Waterlevel Changes in Large Amazon Lake Measured with Space-born Radar Interferometry and Altimetry, *Geophys. Res. Lett.*, 2001, vol. 28, no. 14, pp. 2671–2674.
4. Anzenhofer, M., Shum, C.K., and Rentsh, M., Coastal Altimetry and Applications, *Tech. Rep. ¹ 464. Geodetic Science and Surveying*, The Ohio State University: Columbus, 1999.
5. *AVISO/Altimetry. User Handbook. Merged TOPEX/POSEIDON Products. AVI-NT-02-101-CN. Edition 3.0.* Toulouse: AVISO, 1996.
6. AVISO/Altimetry data center CNES. ftp://avi-softp.cnes.fr
7. Barrick, D., and Lipa, B., Analysis and Interpretation of Altimeter Sea Echo, *Adv. Geophys.*, 1985, vol. 27, pp. 61–100.
8. Berry, P.A.M., Garlick, J.D., Freeman, J.A., and Mathers, E.L., Global Inland Water Monitoring from Multi-Mission Altimetry, *Geophys. Rev. Lett.*, 2005, vol. 32, no. 16.
9. Berry, P.A.M., Smith, R.G., Witheridge, S., and Wheeler, J., Global Inland Water Monitoring from Satellite Radar Altimetry—a Glimpse Into the Future, *ESA Living Planet Symposium*, Bergen, 2010.
10. Birkett, C.M., Mertes, L.A.K., Dunne, T., et al., Surface Water Dynamics in the Amazon Basin: Application of Satellite Radar Altimetry, *J. Geophys. Res.*, 2002, vol. 107, ¹Â 20.
11. Birkett, C.M., Contribution of the Topex NASA Radar Altimeter to the Global Monitoring of Large Rivers and Wetlands, *Water Resour. Res.*, 1998, vol. 34, no. 5, pp. 1223–1239.
12. Brown, G., The Average Impulse Response of a Rough Surface and Its Applications, *Antennas and Propagation*, IEEE Trans, 1977, vol. 25, pp. 67–74.
13. Campos, I.O., Mercier, F., Maheu, C., et al., Temporal Variations of River Basin Waters from Topex/Poseidon Satellite Altimetry. Application to the Amazon Basin, *Earth and Planetary Sciences,* 2001, vol. 333, no. 10, pp. 633–643.
14. Chelton, D.B., Walsh, E.J., and MacArthur J.L., Pulse Compression and Sea Level Tracking in Satellite Altimetry, *J. Atmos. Oceanic Technology*, 1989, vol. 6, no. 3, pp. 407–438.
15. Chelton, D.B., Ries, J.C., Haines, B.J., et al., Satellite Altimetry, *Satellite Altimetry and the Earth Sciences: A Handbook of Techniques and Applications*, L.-L. Fu and A. Cazenave, Eds., San Diego, CA: Academic Press, 2001.
16. Cretaux, J.-F., and Calmant, S., in *Coastal Altimetry*, Vignudelli, S. and Kostianoy, A., Cipollini, P., Benveniste, J., Eds., Berlin: Springer Verlag, 2011, 509–534.
17. Davis, C.H., A Robust Threshold Retracking Algorithm for Measuring Ice Sheet Surface Elevation Change from Satellite Radar Altimeters, *IEEE Trans. Geosci. Remote Sens.*, 1997, vol. 35, no. 4, pp. 974–979.
18. Deng, X., and Featherstone, W.E., A Coastal Retracking System for Satellite Radar Altimeter Waveforms: Application to ERS-2 Around Australia, *J. Geophys. Res.*, 2006, vol. 111, no. C6, pp. 1–16.
19. Donelan, M., Hamilton, J., and Hui, W.H., Directional Spectra of Wind Generated Waves, *Philos. Trans.*

Roy. Soc., London: Ser. A, 1985, vol. A.315, no. 1534, pp. 509–562.

20. Dumont, P., Sicard, P., Stum, J., and Zanife, O.Z., *ADAS Volume 4: CMA Altimeter Level 2 Processing. Issue: 3. Update: 3.* October 18, 2001.
21. Garlick, J.D., Berry, P.A.M., Mathers, E.L., and Benveniste, J., The Envisat/ERS River and Lake Retracking System, *Envisat & ERS symposium proceedings. ESA-SP572, ESA-ESTEC*. Noordwijk, 2004.
22. www.legos.obs-mip.fr/en/soa/hydrologie/hydroweb/General_Info.en.html
23. www.pecad.fas.usda.gov/cropexplorer/global_reservoir/index.cfm)
24. www.ngdc.noaa.gov/mgg/topo/globe.html
25. Koblinsky, C.J., Clarke, R.T., Brenner, A.C., et al., Measurement of River Level Variations with Satellite Altimetry, *Water Resour. Res.,* 1993, vol. 29, no. 6, pp. 1839–1848.
26. Kostyanoi, A.G., Zavialov, P.O., and Lebedev, S.A., What Do We Know About Dead, Dying, and Endangered Lakes and Sea? *Dying and Dead Seas. Climatic Versus Anthropic Causes*, Dordrecht: Kluwer Acad. Publ, 2004, pp. 1–48.
27. Kouraev, A.V., Zakharova, E.A., Samain, O., et al., Ob' River Discharge from TOPEX/Poseidon Satellite Alimetry (1992–2002), *Remote Sensing of Environment,* 2004, vol. 93, nos 1-2, pp. 238–245.
28. Legresy, B., and Remy, F., Using the Temporal Variability of the Radaraltimetric Signal To Map Surface Characteristics of the Antarctic Ice Sheet, *J. of Glaciology*, 1998, vol. 44, no. 147, pp. 197–206.
29. Legresy, B., Papa, F., Remy, F., et al., ENVISAT Radar Altimeter Measurements over Continental Surfaces and Ice Caps Using the ICE-2 Retracking Algorithm, *Remote Sensing of Environment*, 2005, vol. 95, no. 2, pp. 150–163.
30. Maheu, C., Cazenave, A., and Mechoso, C.R., Water Level Fluctuations in the Plata Basin (South America) from Topex/Poseidon Satellite Altimetry, *Geophys. Res. Lett.*, 2003, vol. 30, no. 3, pp. 1143–1146.
31. Martin, T.V., Zwally, H.J., Brenner, A.C., and Bindschadler, R.A., Analysis and Retracking of Continental Ice Sheet Radar Altimeter Waveforms, *J. Geophys. Res.*, 1983, vol. 88, no. C3, pp. 1608–1616.
32. *OSTM/Jason-2 Products Handbook Iss: 1.4 - date: 03*, August 2009.
33. Papa, F., Legresy, B., Mognard, N.M., et al., Estimating Terrestrial Snow Depth with the Topex–Poseidon Altimeter and Radiometer, *IEEE Transactions on Geoscience and Remote Sensing*, 2002, vol. 40, no. 10, pp. 2162–2169.
34. Papa, F., Legresy, B., and Remy, F., Use of the Topex–Poseidon Dualfrequency Radar Altimeter over Land Surfaces, *Remote Sensing of Environment*, 2003, vol. 87, nos. 2-3, pp. 136–147.
35. PODAAC ftp://podaac.jpl.nasa.gov
36. Remy, F., Legresy, B., Bleuzen, S., Vincent, P., and Minster, J.F., Dual-Frequency Topex Altimeter Observation of Greenland, *J. Electron Waves and Aplliance*, 1996, vol. 10, no. 11, pp. 1505–1523.
37. Remy, F., Schaeffer, P., and Legresy, B., Ice Flow Physical Processes Derived from ERS-1 High Resolution Map of the Antarctica and the Greenland Ice Sheets, *Intern. J. of Geophysics*, 1999, vol. 139, no. 3, pp. 645–649.
38. Tournadre, J., Chapron, B., Reul, N., and Vandemark, D.C., Satellite Altimeter Model for Ocean Slick Detection, *J. Geophys. Res.*, 2006, vol. 111, no. C4, p. 22.